

# Effect of iron nanoparticle geometry on the energetics of carbon interstitials

Antti Tolvanen<sup>\*,1</sup>, Arkady V. Krasheninnikov<sup>1,2</sup>, Antti Kuronen<sup>1</sup>, and Kai Nordlund<sup>1</sup>

<sup>1</sup> Division of Material Physics, P.O. Box 43, 00014 University of Helsinki, Finland

<sup>2</sup> Laboratory of Physics, P.O. Box 1100, 02015 Helsinki University of Technology, Finland

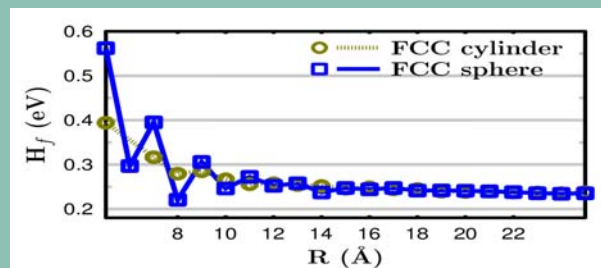
Received 29 May 2009, revised 22 December 2009, accepted 6 January 2010

Published online 4 February 2010

PACS 61.46.Fg, 61.48.-c, 71.15.-m, 81.05.Tp

\* Corresponding author: e-mail antti.tolvanen@helsinki.fi

Understanding the behavior of carbon interstitial atoms in metal nanoparticles is important for a better control over carbon nanotubes growth. Using analytical-potential atomistic simulations, we study the energetics of carbon interstitials in FCC and BCC spherical and cylindrical nano-sized iron particles. An increase in interstitial formation enthalpy (see abstract figure) in small particles gives rise to the reduced solubility of carbon in nanoscale iron. The orientation of interstitial bonds with regard to the nanoparticle surface is shown to have substantial effect on the formation enthalpy. As the radii of the studied systems is reduced below 5 Å the behavior of the interstitial formation energetics become unsystematic.



Formation enthalpies of octahedral and tetrahedral interstitial carbon atoms in FCC and BCC iron is studied by analytical bond order potential. Formation enthalpies are shown to increase with decreasing nanoparticle radius.

© 2010 WILEY-VCH Verlag GmbH & Co. KGaA, Weinheim

**1 Introduction** Carbon nanotubes (CNT) have outstanding electronic and mechanical properties. At the moment, commercial applications of CNTs are mostly limited to materials benefiting from their mechanical properties. The biggest obstacle in the development of applications utilizing the excellent electronic properties of CNTs, and in particular, single walled carbon nanotubes (SWNT), is the lack of control over the growth of SWNTs, as depending on the chirality, the tube can be a metal or semiconductor.

The most widely used growth method of nanotubes is the chemical vapor deposition (CVD) technique where SWNTs precipitate from catalyst metal particles [1–3]. Within the CVD scheme, it is possible to limit the spread of SWNT diameter by catalyst particle size selection [4]. Still, it is not possible to control the chirality of SWNTs, and it seems to be quite unlikely that the controllable growth of

SWNTs can be achieved without the complete understanding of the SWNT growth from metallic nanoparticles.

Widely used model for SWNT growth from metallic nanoparticles is the vapor-liquid-solid model [5,6], in which the growth can be divided into three steps. First carbon precursor molecules are catalytically decomposed on the surface of the catalyst particle. After decomposition the released carbon atoms diffuse into catalytic metal particles. At the final step carbon is precipitated from the metal particles as the solubility limit is reached for the growth temperature and catalyst particle size, or solubility is lowered by changing the temperature.

As the size and shape of catalyst particles may define not only the diameter but also the chirality of the growing tube, it is important to understand how the size effects the solubility and thus optimal synthesis conditions. CVD SWNT growth from C saturated metal particles has been

observed directly in recent *in-situ* transmission electron microscopy (TEM) studies [8,9]. It has also been shown [10] that nanotubes can grow from metal particles inside TEM when carbon atoms sputtered from other carbon nanotubes precipitate on metal particles, which can be referred to as irradiation-mediated self-organization [11]. Very recently it was demonstrated that not only the size of metal particles, but also the geometry affects this process – CNTs precipitated from metal nanoparticles with high curvature [12].

As shown in a recent study [7], carbon solubility is reduced in nanoparticles. The solubility drop was explained in terms of additional pressure in the nanoparticle due to higher surface curvature and thus higher surface energy. However, it was assumed that the geometry of the particle is spherical, and the actual atomic structures of the particles, surface orientations etc. were not taken into account. In this work, we try to address these issues by directly simulating metal nanoparticles of different sizes and geometries with carbon interstitials for both minimum and saddle point configurations of the interstitials.

**2 Simulation method** We used a recently developed analytical bond-order potential to model Fe-C systems [19]. The potential has been successfully fitted to cementite and Hägg carbide, which are most important crystalline polytypes among the many known metastable iron carbide phases. Predicted properties of other carbides and the simplest point defects are in good to reasonable agreement with available data from experiments and density-functional theory calculations. The potential correctly describes melting and recrystallization of cementite, and being much more computationally efficient than first-principle simulations, makes it possible to study large systems composed up to million atoms.

As the actual geometry of catalytic particles is unknown, three different types of systems were studied: spherical nanoparticles of radii up to 70 Å and number of atoms from a few to ~ 75000, nanorods with radii to to 40 Å and up to ~ 35000 atoms, and semi-infinite slabs. All systems were studied in FCC ( $\gamma$ -Fe, austenite) and BCC ( $\alpha$ -Fe, ferrite) phases. Both phases were studied as both structures are observed in metal nanoparticles, FCC being the more common. Theoretically, the FCC phase has been claimed to be the lowest-energy state of nanoparticles after the number of atoms is reduced below a material dependent limit [13,14]. Spherical nanoparticles and cylinders were formed by cutting the system from FCC or BCC bulk lattice with the selected radii. After geometry optimization these systems acquired realistically faceted structures due to the minimization of the surface energy. For pure Fe systems the final energies per atom were almost identical to those given by test system formed as Wulff polyhedra. Slabs with periodic boundaries in two directions were used to study the dependence of carbon interstitial formation

enthalpy as a function of the distance to BCC 110 and FCC 100 surfaces.

Systems were relaxed using conjugate gradient method leading to the zero temperature minimum energy configuration using our `Relaxat` code [15]. Control runs performed with molecular dynamics simulations where the systems were annealed at 500 K temperature for 50 fs using the `PARCAS` code [16] gave similar results.

Defect formation enthalpy  $H_f$  was calculated from:

$$H_f = E_{Fe+C} - E_{Fe} - E_{graphene}, \quad (1)$$

where  $E_{graphene}$  is the energy per atom in graphene and  $E_{Fe+C}$  and  $E_{Fe}$  are the energies of the system with/without C interstitial. As the energy of an isolated C atom is zero in our model,  $E_{graphene} = 7.375$  eV/atom coincided with the cohesive energy of graphene.

**3 Results and discussion** An interstitial C atom in Fe BCC or FCC lattice can be in either an octahedral or tetrahedral position. The atomic structures of these defects are presented in Fig. 1. The octahedral position is both for FCC and BCC lattices the lowest energy configuration for the interstitial position.

Bulk FCC and BCC has 4 and 6 octahedral and 8 and 12 tetrahedral interstitial positions in the unit cell, respectively. Even though in bulk systems all octahedral and tetrahedral positions are equivalent, the situation can change substantially in a finite system. In a small particle, the direction of the orthogonal bonds of octahedral interstitial with respect to the surface directions of will change the otherwise equivalent interstitial positions and cause changes in the formation enthalpy. For tetrahedral positions the changes are smaller as tetrahedral interstitials have bonds in all three spatial planes compared to the two planes of octahedral bonding.

The formation enthalpies for bulk interstitials calculated by Eq. (1) are presented in Table 1. As compared to *ab initio* results [17] 0.70 eV and 1.80 eV for octahedral and tetrahedral formation enthalpies in BCC iron, respectively, our method gives higher enthalpy for octahedral interstitial formation. On the other hand *ab initio* density functional theory computations can even give negative values for these enthalpies [18]. Besides, we concentrate on relative values related to the changes in the size of the system.

**Table 1** Formation enthalpies of C interstitials for octahedral and tetrahedral configurations in bulk FCC and BCC iron and energy difference between the configurations.

Lattice	Octahedral	Tetrahedral	$\Delta E$
FCC	0.24 eV	1.01 eV	0.77 eV
BCC	1.27 eV	1.81 eV	0.54 eV

Resulting difference between octahedral and tetrahedral interstitial formation enthalpies  $\Delta E$  in the BCC is slightly underestimated compared to experimental values

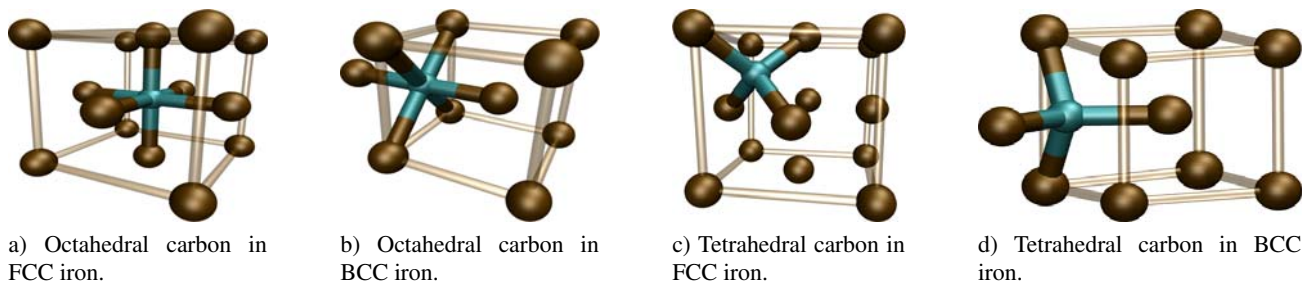


**Figure 1** Octa- and tetrahedral interstitial sites in FCC and BCC iron.

0.88 eV [21] and 0.84 eV [20]. For FCC the formation enthalpy of octahedral interstitial is also underestimated compared to experimental value of 0.4 eV. For both FCC and BCC, we find the correct octahedral minimum energy configuration. In conclusion the method used is in reasonable agreement with previous experimental and computational results (for more details see [19]).

**3.1 Spherical nanoparticles** Spherical nanoparticles were studied as the simplest case of a metal nanoparticle relevant to carbon-metal nanosystems [22,23]. Carbon interstitial was positioned at the center of the sphere. In all studied cases, the interstitial bond directions relaxed into the minimal configuration with respect to the surface facets. The atomic configurations are presented in Fig. 2. The formation enthalpy increases systematically when

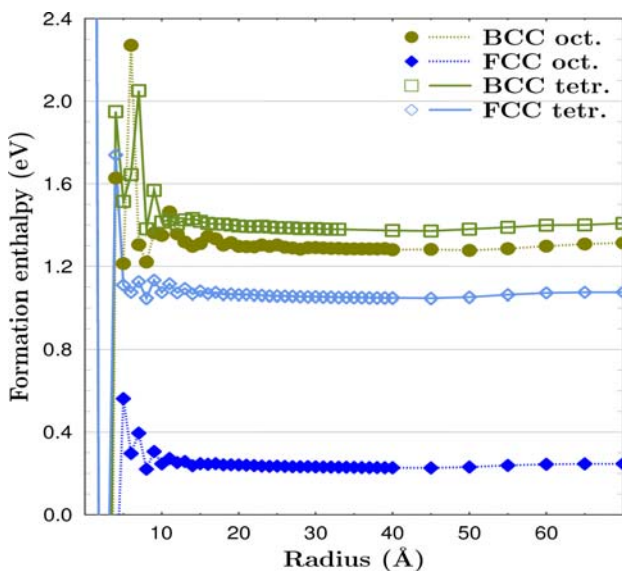


**Figure 2** Carbon interstitial formation enthalpies in Fe spherical nanoparticles as a function of nanoparticle radius.

the radius decreases from 40 Å to 6 Å, see Fig. 2. For small radii of the particles, the behavior becomes non-monotonous due to large changes in the atomic configuration and direct interaction of the interstitial with under-

coordinated surface atoms. As the radius increases the enthalpy approaches the bulk value of the respective system. The difference in octahedral and tetrahedral interstitial formation enthalpies stays constant in FCC systems except for systems with small radii in contrast to the BCC systems where this difference reduces after 20 Å radius and finally tetrahedral configuration becomes the lowest energy configuration at 11 Å radius. It can be concluded that the vicinity of the surface reduces the difference between the lowest energy and saddle point enthalpies. Similar results have been reported before by Abild-Pedersen et al. in [24], where graphene growth from nickel nanoparticles was studied using *ab initio* density functional theory calculations. They show that diffusion energy barrier can be ~50% lower in the subsurface layer than in bulk.

**3.2 Nanorods** Iron nanorods (see e.g. [25] for carbide and [26,27] for carbon encapsulated nanorods) were simulated. The nanorod radii were up to 40 Å. The length of the cylinders carved from BCC and FCC bulk iron was much longer than the radius. The systems were centered on the carbon interstitial placed on such position that after relaxation the interstitial was on octahedral or tetrahedral site in the center of the rod. Various lattice directions of nanorod axis were studied. The results for FCC 100, 110 and BCC 100 axial directions are presented in Fig. 3. Also 121, 100 and 101 axial directions were studied, giving results similar to the presented.

Octahedral carbon interstitial, Fig. 1(b), is bonded to six Fe atoms from which four of Fe atoms are located on the same plane. In our simulations of the nanosystems the two off-plane Fe atoms were displaced more than the planar atoms of the defect. This geometrical effect can be seen from BCC100 oct.1 and BCC100 oct.2 data in Fig. 3, where the off-plane atoms of the defect are aligned axially and radially, respectively. Such effect naturally can not be seen in the results for spherical nanoparticles because of the radial symmetry.

**3.3 Interstitial near the surface of bulk systems** Octahedral interstitial formation was simulated in FCC and BCC slab systems in order to obtain information of the effect of vicinity of the surface in bulk systems. A slab of ~40 Å length in non-periodic direction was used allowing maximum interstitial depth of 20 Å. The re-

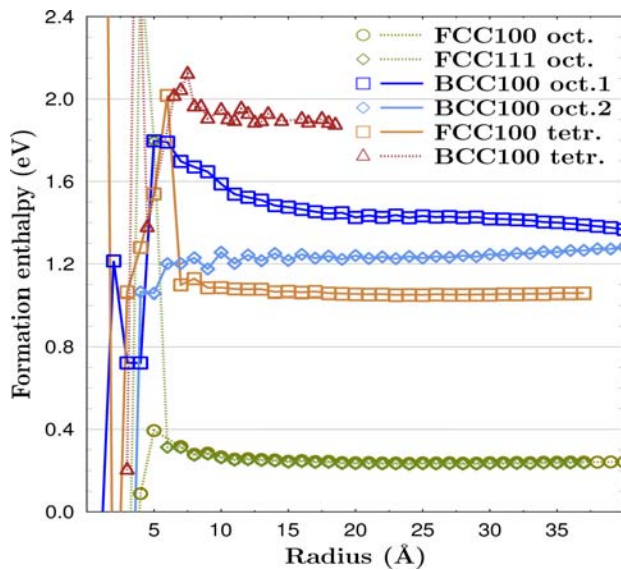


**Figure 3** Carbon interstitial formation enthalpies in Fe nanorods as a function of nanorod radius. For BCC rods both perpendicular (1) and parallel (2) octahedral interstitial configurations are considered.

sults are presented in Fig. 4. For BCC system two values above the surface are presented, the lower corresponds to the bridge position and the higher to the top position of C atom.

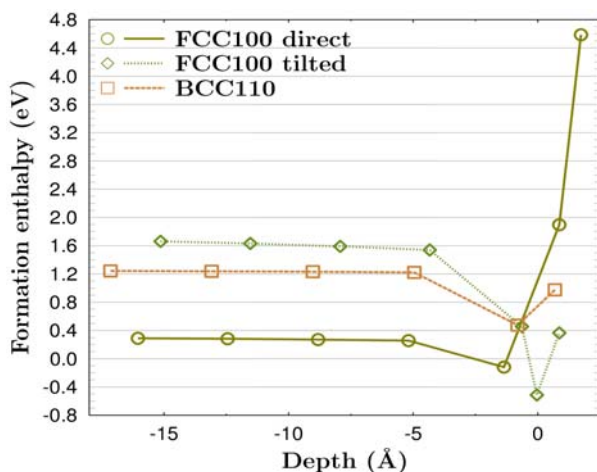


**Figure 4** Octahedral interstitial formation enthalpies of C in BCC and FCC slab systems as a function of interstitial depth from the surface. The surface is located at 0 depth, positive direction away from the surface.

For FCC100 surface two different octahedral interstitial orientations were found. In the direct orientation the bonds of octahedral defect are oriented perpendicular and parallel directions with the surface and in tilted direction the planar Fe atoms of the defect are in 111 plane. In this

orientation the most displaced atoms of the defect are displaced in the direction forming an angle of  $\frac{\pi}{4}$  radians with respect the surface vector. In our results there was a decrease of the interstitial formation enthalpy in the vicinity of the flat surface. Similar results have been reported before for other metal catalysts [28] It can be seen from the results that the used slab thickness did not allow the formation enthalpy to reach the bulk value even at the maximum depth allowed by the simulated system.

**4 Conclusions** Our simulations show that in small cylindrical nanorods and spherical iron nanoparticles, the formation enthalpy of carbon interstitial is increased due to extra pressure induced by the surface curvature leading to a decrease in carbon solubility. This result holds unless the system becomes very small, about few lattice constant of the material, when the interstitial is bonded directly to the surface atoms.

In nano-sized systems the octahedral interstitial positions are not equivalent and the formation enthalpy depends on the separation of the interstitial from the surface and the orientation of the defect with regard to the surface of the system. Our results indicate that solubility of carbon in small particles is indeed reduced and that precipitation of carbon nanotubes is more likely at small particles with a high radius of surface curvature.

**Acknowledgements** This work was supported by the Academy of Finland under CONADEP, OPNA projects, and the Centre of Excellence program. We are also indebted to the Finnish IT Center for Science for generous grants of computer time. AVK acknowledges support from the European Commission under the 6th Framework Programme STREP (Project BNC Tubes, Contract No. NMP4-CT-2006-033350).

## References

- [1] A. Thess, R. Lee, P. Nikolaev, H. Dai, P. Petit, J. Robert, C. Xu, Y. H. Lee, S. Gon Kim, A. G. Rinzler, D. T. Colbert, G. E. Scuseria, D. Tomnek, J. E. Fischer, Richard E. Smalley, *Science* **273**, 483 (1996).
- [2] L. Ci, Y. Li, B. Wei, J. Liang, C. Xu, D. Wu, *Carbon* **38**, 1933 (2000).
- [3] H. W. Zhu, C. L. Xu, D. H. Wu, B. Q. Wei, R. Vajtai, and P. M. Ajayan, *Science* **296**, 884 (2002).
- [4] C. L. Cheung, A. Kurtz, H. Park, and C. M. Lieber, *J. Phys. Chem. B* **106**, 2429 (2002).
- [5] Y. Saito, *Carbon* **33**, 979 (1995).
- [6] J. Gavillet, A. Loiseau, C. Journet, F. Willaime, F. Ducastelle, and J.-C. Charlier, *Phys. Rev. Lett.* **87**, 275504 (2001)
- [7] A. R. Harutyunyan, N. Awasthi, A. Jiang, W. Setyawan, E. Mora, T. Tokune, K. Bolton, and S. Curtarolo, *Phys. Rev. Lett* **100**, 195502 (2008).
- [8] S. Hofmann, R. Sharma, C. Ducati, G. Du, C. Mattevi, C. Cepek, M. Cantoro, S. Pisana, A. Parvez, F. Cervantes-Sodi, A. C. Ferrari, R. Dunin-Borkowski, S. Lizzit, L. Petaccia, A. Goldoni, and J. Robertson, *Nano Lett* **7**, 602 (2007).

- [9] S. Helveg, C. Lopez-Cartes, J. Sehested, P. L. Hansen, B. S. Clausen, J. R. Rostrup-Nielsen, F. Abild-Pedersen, and J. K. Nørskov *Nature* **427**, 426 (2004).
- [10] J. A. Rodríguez-Manzo, M. Terrones, H. Terrones, H. W. Kroto, L. Sun, F. Banhart, *Nature Nanotechnol.* **2**, 307 - 311 (2007).
- [11] A. V. Krasheninnikov and F. Banhart, *Nature Mater.* **6**, 723 (2007).
- [12] J. A. Rodríguez-Manzo, I. Janowska, C. Pham-Huu, A. Tolvanen, A. V. Krasheninnikov, K. Nordlund, and F. Banhart, *Small* **5**, 2710 (2009).
- [13] D. Tománek, S. Mukherjee and K. H. Bennemann, *Phys. Rev. B* **28**, 665 (1983).
- [14] S. H. Huh, H. K. Kim, J. W. Park, and G. H. Lee, *Phys. Rev. B* **62**, 2937 (2000).
- [15] K. Nordlund, P. Partyka, and R. S. Averback, in: *Defects and Diffusion in Silicon Processing*, Vol. 469 of MRS Symposium Proceedings, edited by T. Diaz de la Rubia and S. Coffa (Materials Research Society, Pittsburgh, 1997), p. 199.
- [16] PARCAS code by K. Nordlund (2009).
- [17] C. Domain, C. S. Becquart, and J. Foct, *Phys. Rev. B* **69**, 144112 (2004).
- [18] D. E. Jiang and E. A. Carter, *Phys. Rev. B* **67**, 214103 (2003).
- [19] K. O. E. Henriksson and K. Nordlund, *Phys. Rev. B* **79**, 144107 (2009).
- [20] R. B. McLellan and M. L. Wasz, *J. Phys. Chem. Solids* **54**, 583 (1993).
- [21] S. Takaki, J. Fuss, H. Kugler, U. Dedek, and H. Schultz, *Radiat. Eff.* **79**, 87 (1983)
- [22] L. Sun, A. V. Krasheninnikov, T. Ahlgren, K. Nordlund, and F. Banhart, *Phys. Rev. Lett.* **101**, 156101 (2008).
- [23] H. Zhu, K. Suenaga, A. Hashimoto, K. Urita, K. Hata, and S. Iijima, *Small* **1**, 1180 (2005).
- [24] F. Abild-Pedersen et al., *Phys. Rev. B* **73**, 115419 (2006).
- [25] H. Dai, E. W. Wong, Y. Z. Lu, S. Fan, and C. M. Lieber, *Nature* **375**, 769 (1995).
- [26] L. Sun, F. Banhart, A. V. Krasheninnikov, J. A. Rodríguez-Manzo, M. Terrones, and P. M. Ajayan, *Science* **312**, 1199 (2006).
- [27] J. Huo, H. Song, X. Chen, and B. Cheng, *J. Phys. Chem. C* **112**, 5835 (2008).
- [28] O. V. Yazyev and A. Pasquarello, *Phys. Rev. Lett* **100**, 156102 (2008) and *Phys. Status Solidi B* **245**, 2158 (2008).